Supplementary Table S1. CD3-binding properties of 4B1, OKT3 and UCHT1 antibodies

Antibody (mAb)	Affinity of mAb to TCR-CD3 protein *K*d（nM）	Extent of CD69 (%)
UCHT1	< 0.001	93.5
OKT3	0.175	82.2
4B1	0.027	89.5

Supplementary Table S2. Cryo-EM data collection, refinement and validation statistics

	TCR-CD3-4B1	TCR-CD3-OKT3
Data collection and processing		
Magnification	96,000	215,000
Voltage (kV)	300	300
Electron exposure (e^{-}/Å^2)	40.0	60.0
Defocus range (μm)	−1.5 to 2.5	−1.5 to 2.5
Pixel size (Å)	0.86	0.335
Symmetry imposed	C1	C1
Initial particle images (no.)	2,921,005	5,496,886
Final particle images (no.)	439,348	502,960
Map resolution (Å)	3.14	3.18
FSC threshold	0.143	0.143
Map resolution range (Å)	6.00-3.14	6.00-3.18
Refinement		
Initial model used (PDB code)	6JXR	6JXR
Model resolution (Å)	3.14	3.18
FSC threshold	(0.143)	(0.143)
Model resolution range (Å)	6.00-3.14	6.00-3.18
Map sharpening *B* factor (Å^2)	−129.1	-137.9
Model composition		
Nonhydrogen atoms	11692	14988
Protein residues	1495	1922
CLR	2	2
B factors (Å^2)		
Protein	183.37	50.15
CLR	56.61	48.25
R.m.s. deviations		
Bond lengths (Å)	0.007	0.003
Bond angles (°)	1.068	0.825
Validation		
MolProbity score	1.70	1.61
Clashscore	4.93	5.45
Poor rotamers (%)	0.38	0.06
Ramachandran plot		
Favored (%)	93.08	95.52
Allowed (%)	6.92	4.48
Disallowed (%)	0.00	0.00

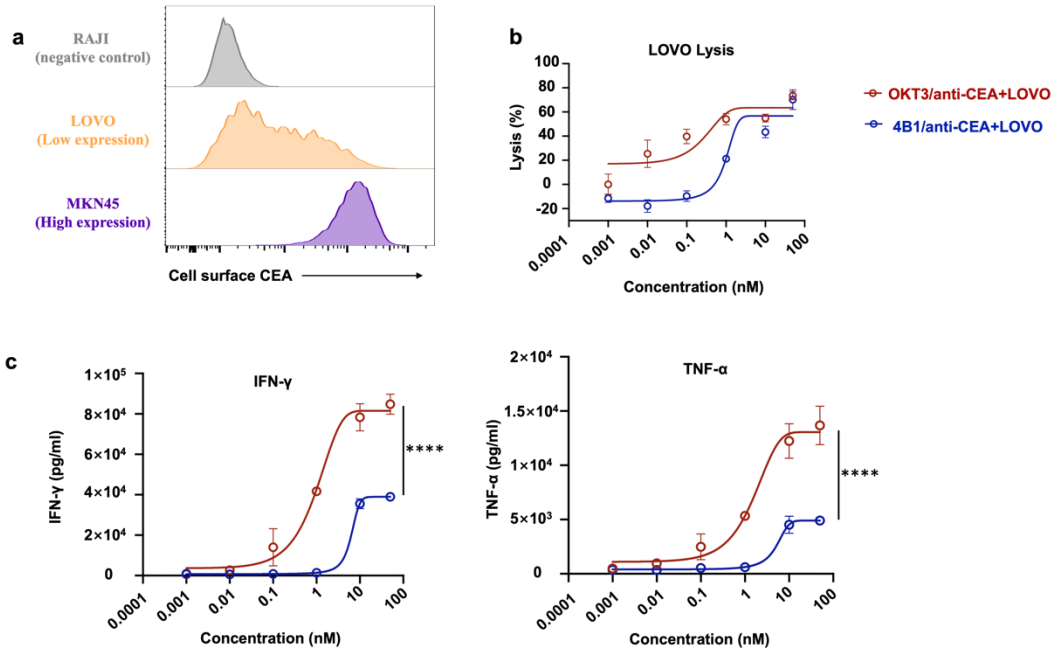

Supplementary Fig.S1 4B1-based bispecific antibody maintains potent tumor killing under low antigen density with minimal cytokine release

a Representative flow cytometry histogram showing surface expression of carcinoembryonic antigen CEA on RAJI (negative control), LOVO (low expression), and MKN45 (high expression) cell lines.

b Dose-dependent killing of CEA-low LOVO cells by human T cells pre-incubated with OKT3/anti-CEA or 4B1/anti-CEA bispecific antibodies (E:T ratio = 10:1, 48 h). Data are presented as mean ± SEM, $n = 3$.

c Levels of IFN-γ and TNF-α released into the supernatant during the co-culture in b. Data are presented as mean ± SEM, n = 3. Statistical significance was calculated with two-way ANOVA: ****P < 0.0001.

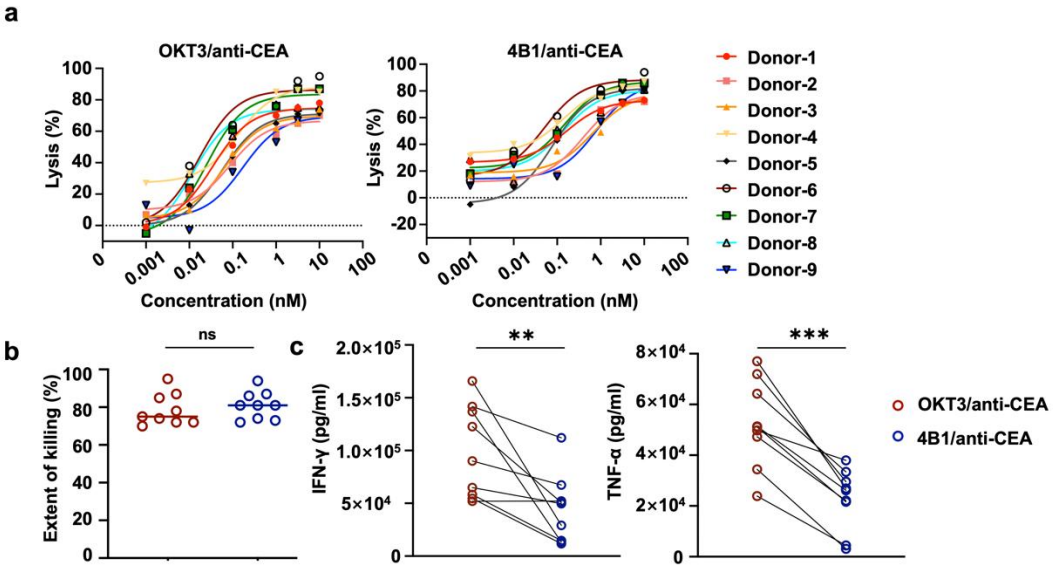

Supplementary Fig.S2 4B1 BsAbs-mediated tumor cell killing activity and cytokine release by primary PBMCs from healthy donors

a Levels of tumor cell lysis were measured following the isolation of human PBMCs from 9 different healthy donors. Subsequently, these PBMCs were incubated with MKN45 tumor cells (at a 10:1 cell ratio) and various concentrations of CD3/anti-CEA antibodies for 24 h.

b For dot plots, the extent of killing is reported, and each dot represents a unique donor with a horizontal bar indicating the mean. Statistical significance was calculated with paired Student's *t*-test.

c Measurement of IFN-γ and TNF-α cytokine levels of cells treated as in **(a)** incubation conditions. Data are presented as mean ± SEM, $n = 9$. Statistical significance was calculated with a paired Student's *t*-test. OKT3/anti-CEA versus 4B1/anti-CEA: $^{**}P < 0.01$ and $^{***}P < 0.001$.

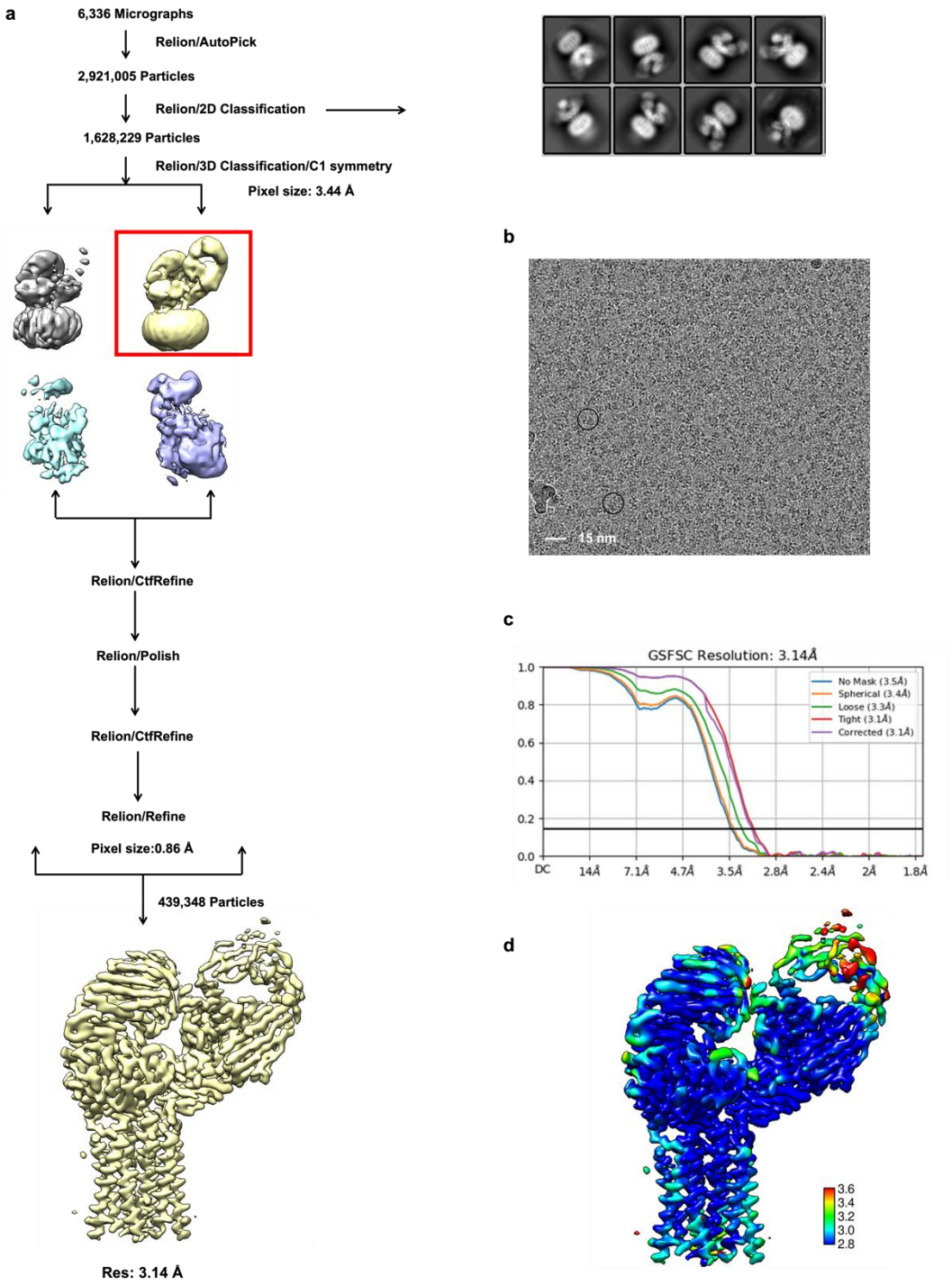

Supplementary Fig.S3 Cryo-EM image processing procedure of the TCR-CD3-4B1 complex

a Image processing workflow of the TCR–CD3–4B1 complex.

b A representative raw cryo-EM image of the TCR–CD3–4B1 complex. The particles that were picked for classification are labeled with circles.

c Gold standard FSC plot for the final 3D reconstruction of the TCR–CD3–4B1 complex.

d Resolution map for the final 3D reconstruction of the TCR–CD3–4B1 complex. The color code for resolutions, shown with the unit Å, is calculated using cryoSPARC.

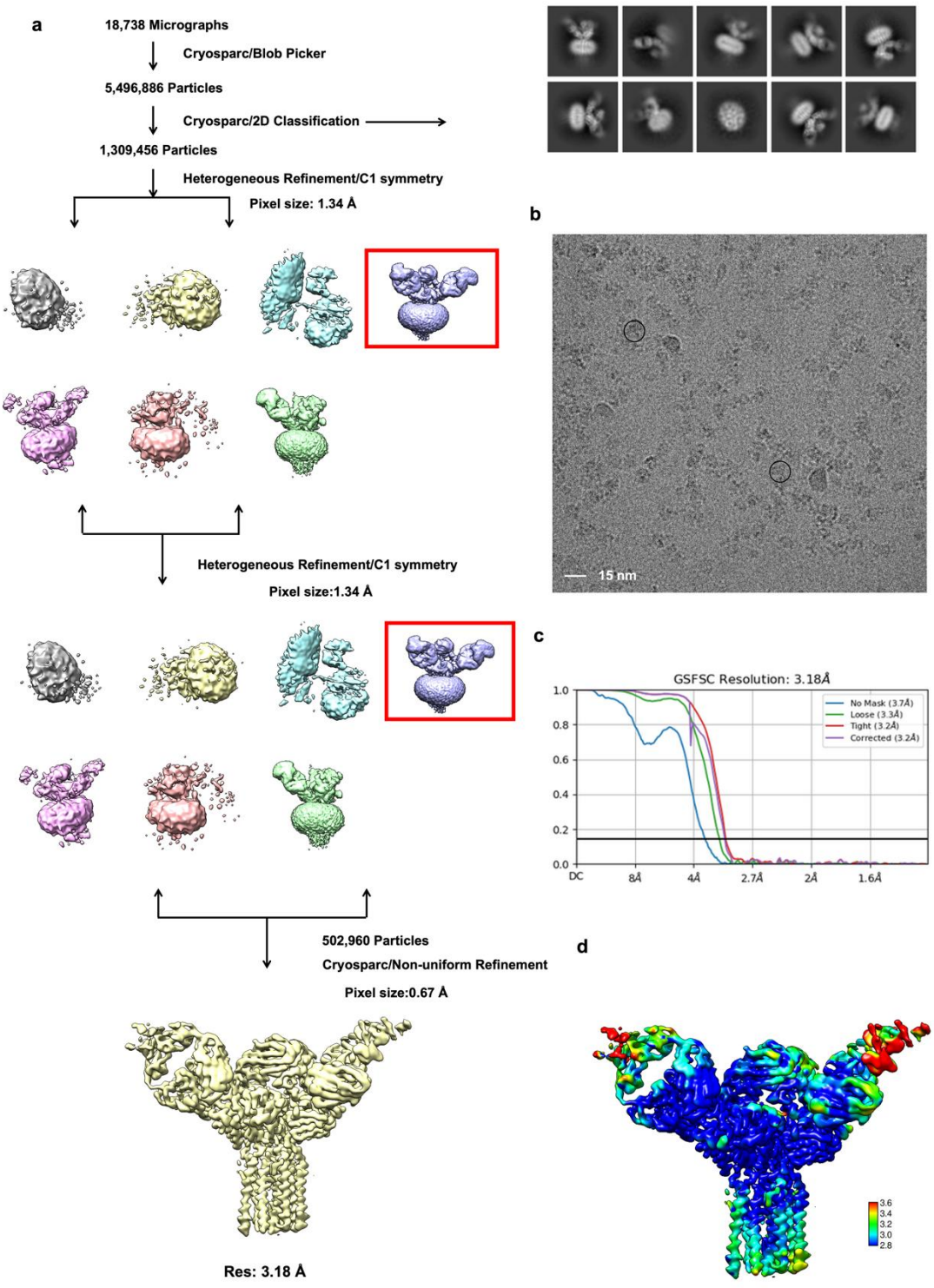

Supplementary Fig.S4 Cryo-EM image processing procedure of the TCR-CD3-OKT3 complex

a Image processing workflow of the TCR–CD3–OKT3 complex.

b A representative raw cryo-EM image of the TCR–CD3–OKT3 complex. The particles that were picked for classification are labeled with circles.

c Gold standard FSC plot for the final 3D reconstruction of the TCR–CD3–OKT3 complex.

d Resolution map for the final 3D reconstruction of the TCR–CD3–OKT3 complex. The color code for resolutions, shown with the unit Å, is calculated using cryoSPARC.

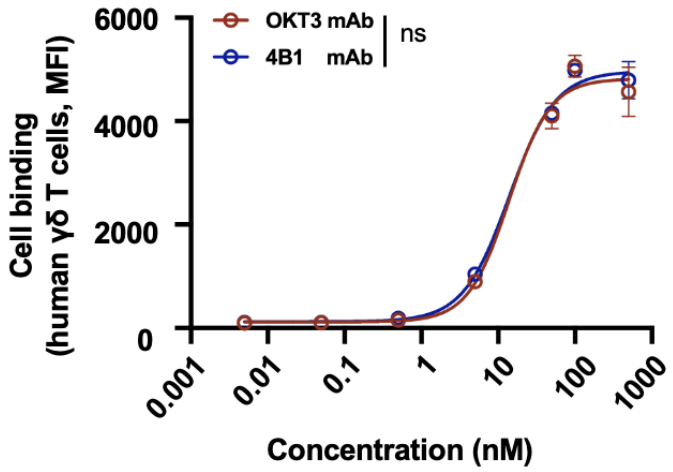

Supplementary Fig.S5 Binding of OKT3 and 4B1 mAbs to primary human γδ T cells

1×10^7/mL purified human γδ T cells were incubated for 30 min with increasing doses of OKT3 and 4B1 mAbs. The cells were then labeled with anti-human IgG-FITC secondary antibodies. The MFI of antibody binding to human T cells was detected by flow cytometry dependent on antibody concentrations. Data are presented as mean ± SEM, n = 3. Statistical significance was calculated with two-way ANOVA: ns, not significant.

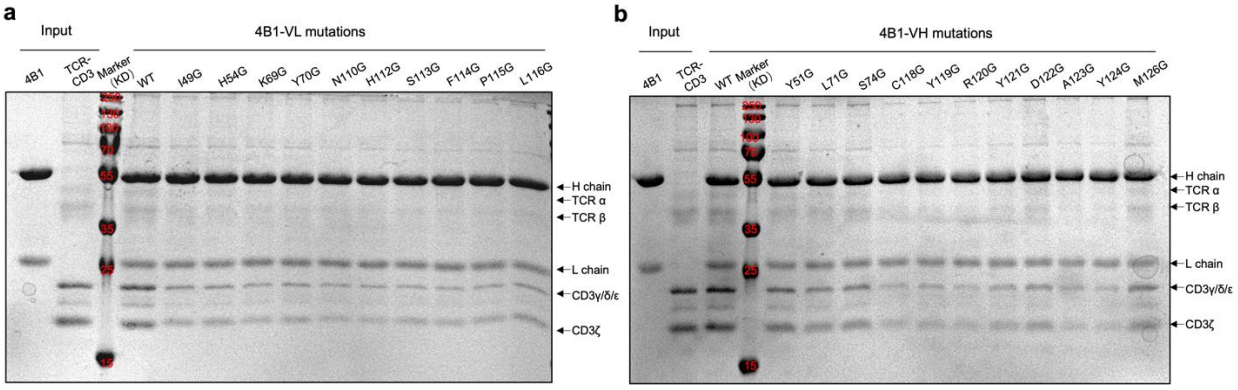

Supplementary Fig. S6. TCR-CD3 pull-down experiments with 4B1 variants

Representative coomassie blue-stained SDS-PAGE gels showing TCR–CD3 complex co-immunoprecipitation with wild-type (WT) and mutant 4B1 variants: light-chain (vL) mutants (**a**) and heavy-chain (vH) mutants (**b**). The positions of the TCR-CD3 complex, 4B1 heavy chain (H chain), and 4B1 light chain (L chain) are indicated. Relative band intensities were quantified and normalized to WT 4B1 to generate the bar graphs presented in Fig. 5d.

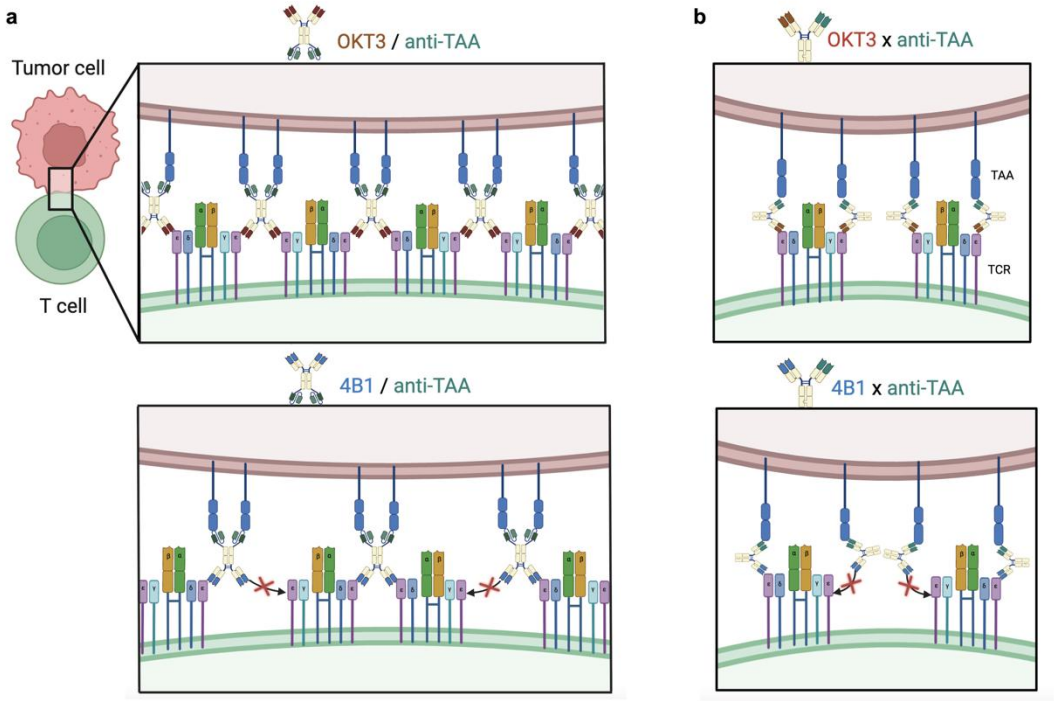

Supplementary Fig. S7. A model figure depicting distinct avidity mechanisms of IgG-scFv versus CrossMab bispecific antibodies

a-b TCR interaction with IgG-scFv (**a**) versus CrossMab (**b**) bispecific antibodies. For simplicity, the schematic diagram hides the CD3ζ/ζ' subunits.